Biomedical Optics EXPRESS

Noninvasive diffuse optical monitoring of head and neck tumor blood flow and oxygenation during radiation delivery

Lixin Dong,[1] Mahesh Kudrimoti,[2] Ran Cheng,[1] Yu Shang,[1] Ellis L. Johnson,[2] Scott D. Stevens,[3] Brent J. Shelton,[4] and Guoqiang Yu[1,*]

[1]*Center for Biomedical Engineering, University of Kentucky College of Engineering, Lexington, KY 40506, USA*
[2]*Department of Radiation Medicine, University of Kentucky Chandler Hospital, Lexington, KY 40536, USA*
[3]*Department of Radiology, University of Kentucky Chandler Hospital, Lexington, KY 40536, USA*
[4]*Markey Cancer Center, University of Kentucky College of Medicine, and Department of Biostatistics, University of Kentucky College of Public Health, Lexington, KY 40536, USA*
**guoqiang.yu@uky.edu*

Abstract: This study explored using a novel diffuse correlation spectroscopy (DCS) flow-oximeter to noninvasively monitor blood flow and oxygenation changes in head and neck tumors during radiation delivery. A fiber-optic probe connected to the DCS flow-oximeter was placed on the surface of the radiologically/clinically involved cervical lymph node. The DCS flow-oximeter in the treatment room was remotely operated by a computer in the control room. From the early measurements, abnormal signals were observed when the optical device was placed in close proximity to the radiation beams. Through phantom tests, the artifacts were shown to be caused by scattered x rays and consequentially avoided by moving the optical device away from the x-ray beams. Eleven patients with head and neck tumors were continually measured once a week over a treatment period of seven weeks, although there were some missing data due to the patient related events. Large inter-patient variations in tumor hemodynamic responses were observed during radiation delivery. A significant increase in tumor blood flow was observed at the first week of treatment, which may be a physiologic response to hypoxia created by radiation oxygen consumption. Only small and insignificant changes were found in tumor blood oxygenation, suggesting that oxygen utilizations in tumors during the short period of fractional radiation deliveries were either minimal or balanced by other effects such as blood flow regulation. Further investigations in a large patient population are needed to correlate the individual hemodynamic responses with the clinical outcomes for determining the prognostic value of optical measurements.

OCIS codes: (170.0170) Medical optics and biotechnology; (170.3660) Light propagation in tissues; (170.3880) Medical and biological imaging; (170.6480) Spectroscopy, speckle.

References and links

1. R. I. Haddad, *Multidisciplinary Management of Head and Neck Cancer* (Demos Medical, New York, 2011).
2. NCI, "Head and Neck Cancer: Questions and Answers" (National Cancer Institute, 2005), retrieved Oct. 24 2011, http://www.cancer.gov/cancertopics/factsheet/Sites-Types/head-and-neck.
3. B. Kwabi-Addo and T. L. Lindstrom, *Cancer Causes and Controversies: Understanding Risk Reduction and Prevention* (Praeger, Santa Barbara, Calif., 2011).
4. J. Bernier and S. M. Bentzen, "Radiotherapy for head and neck cancer: latest developments and future perspectives," Curr. Opin. Oncol. **18**(3), 240–246 (2006).
5. R. E. Lenhard, R. T. Osteen, T. S. Gansler, and American Cancer Society, *Clinical Oncology*, 1st ed. (American Cancer Society, Atlanta, Ga., 2001).

#157289 - $15.00 USD Received 28 Oct 2011; revised 15 Dec 2011; accepted 1 Jan 2012; published 4 Jan 2012

6. E. J. Hall and A. J. Giaccia, *Radiobiology for the Radiologist*, 6th ed. (Lippincott Williams & Wilkins, Philadelphia, 2006).
7. V. T. DeVita, T. S. Lawrence, and S. A. Rosenberg, *DeVita, Hellman, and Rosenberg's Cancer: Principles & Practice of Oncology*, 9th ed. (Wolters Kluwer Health/Lippincott Williams & Wilkins, Philadelphia, 2011).
8. R. A. Gatenby, H. B. Kessler, J. S. Rosenblum, L. R. Coia, P. J. Moldofsky, W. H. Hartz, and G. J. Broder, "Oxygen distribution in squamous cell carcinoma metastases and its relationship to outcome of radiation therapy," Int. J. Radiat. Oncol. Biol. Phys. **14**(5), 831–838 (1988).
9. M. Nordsmark, M. Overgaard, and J. Overgaard, "Pretreatment oxygenation predicts radiation response in advanced squamous cell carcinoma of the head and neck," Radiother. Oncol. **41**(1), 31–39 (1996).
10. D. M. Brizel, G. S. Sibley, L. R. Prosnitz, R. L. Scher, and M. W. Dewhirst, "Tumor hypoxia adversely affects the prognosis of carcinoma of the head and neck," Int. J. Radiat. Oncol. Biol. Phys. **38**(2), 285–289 (1997).
11. H. Lyng, G. Tanum, J. F. Evensen, E. K. Rofstad, H. Lyng, G. Tanum, and J. F. Ev, "Changes in oxygen tension during radiotherapy of head and neck tumours," Acta Oncol. **38**(8), 1037–1042 (1999).
12. H. Lyng, K. Sundfør, and E. K. Rofstad, "Changes in tumor oxygen tension during radiotherapy of uterine cervical cancer: relationships to changes in vascular density, cell density, and frequency of mitosis and apoptosis," Int. J. Radiat. Oncol. Biol. Phys. **46**(4), 935–946 (2000).
13. N. A. Mayr, W. T. Yuh, V. A. Magnotta, J. C. Ehrhardt, J. A. Wheeler, J. I. Sorosky, C. S. Davis, B. C. Wen, D. D. Martin, R. E. Pelsang, R. E. Buller, L. W. Oberley, D. E. Mellenberg, and D. H. Hussey, "Tumor perfusion studies using fast magnetic resonance imaging technique in advanced cervical cancer: a new noninvasive predictive assay," Int. J. Radiat. Oncol. Biol. Phys. **36**(3), 623–633 (1996).
14. D. M. Brizel, R. K. Dodge, R. W. Clough, and M. W. Dewhirst, "Oxygenation of head and neck cancer: changes during radiotherapy and impact on treatment outcome," Radiother. Oncol. **53**(2), 113–117 (1999).
15. R. Hermans, P. Lambin, A. Van der Goten, W. Van den Bogaert, B. Verbist, C. Weltens, and P. R. Delaere, "Tumoural perfusion as measured by dynamic computed tomography in head and neck carcinoma," Radiother. Oncol. **53**(2), 105–111 (1999).
16. A. F. DeVries, C. Kremser, P. A. Hein, J. Griebel, A. Krezcy, D. Ofner, K. P. Pfeiffer, P. Lukas, and W. Judmaier, "Tumor microcirculation and diffusion predict therapy outcome for primary rectal carcinoma," Int. J. Radiat. Oncol. Biol. Phys. **56**(4), 958–965 (2003).
17. R. Hermans, M. Meijerink, W. Van den Bogaert, A. Rijnders, C. Weltens, and P. Lambin, "Tumor perfusion rate determined noninvasively by dynamic computed tomography predicts outcome in head-and-neck cancer after radiotherapy," Int. J. Radiat. Oncol. Biol. Phys. **57**(5), 1351–1356 (2003).
18. M. J. Mäntylä, J. T. Toivanen, M. A. Pitkänen, and A. H. Rekonen, "Radiation-induced changes in regional blood flow in human tumors," Int. J. Radiat. Oncol. Biol. Phys. **8**(10), 1711–1717 (1982).
19. K. Lehtiö, O. Eskola, T. Viljanen, V. Oikonen, T. Grönroos, L. Sillanmäki, R. Grénman, and H. Minn, "Imaging perfusion and hypoxia with PET to predict radiotherapy response in head-and-neck cancer," Int. J. Radiat. Oncol. Biol. Phys. **59**(4), 971–982 (2004).
20. S. L. Bacharach, S. K. Libutti, and J. A. Carrasquillo, "Measuring tumor blood flow with H(2)(15)O: practical considerations," Nucl. Med. Biol. **27**(7), 671–676 (2000).
21. A. Ishii, Y. Korogi, R. Nishimura, K. Kawanaka, M. Yamura, I. Ikushima, T. Hirai, Y. Yamashita, and M. Shinohara, "Intraarterial infusion chemotherapy for head and neck cancers: evaluation of tumor perfusion with intraarterial CT during carotid arteriography," Radiat. Med. **22**(4), 254–259 (2004).
22. W. C. Yang, V. Shah, M. Nussbaum, and J. G. Sarlin, "Desmoid tumor of the neck: CT and angiographic findings," AJNR Am. J. Neuroradiol. **5**(4), 478–480 (1984).
23. M. Rijpkema, J. H. Kaanders, F. B. Joosten, A. J. van der Kogel, and A. Heerschap, "Effects of breathing a hyperoxic hypercapnic gas mixture on blood oxygenation and vascularity of head-and-neck tumors as measured by magnetic resonance imaging," Int. J. Radiat. Oncol. Biol. Phys. **53**(5), 1185–1191 (2002).
24. R. S. Sawaqed, F. J. Podbielski, H. E. Rodriguez, I. M. Wiesman, M. M. Connolly, and E. T. Clark, "Prospective comparison of intraoperative angiography with duplex scanning in evaluating lower-extremity bypass grafts in a community hospital," Am. Surg. **67**(6), 601–604 (2001).
25. G. Yu, T. Durduran, C. Zhou, H. W. Wang, M. E. Putt, H. M. Saunders, C. M. Sehgal, E. Glatstein, A. G. Yodh, and T. M. Busch, "Noninvasive monitoring of murine tumor blood flow during and after photodynamic therapy provides early assessment of therapeutic efficacy," Clin. Cancer Res. **11**(9), 3543–3552 (2005).
26. T. Durduran, R. Choe, G. Yu, C. Zhou, J. C. Tchou, B. J. Czerniecki, and A. G. Yodh, "Diffuse optical measurement of blood flow in breast tumors," Opt. Lett. **30**(21), 2915–2917 (2005).
27. U. Sunar, H. Quon, T. Durduran, J. Zhang, J. Du, C. Zhou, G. Yu, R. Choe, A. Kilger, R. Lustig, L. Loevner, S. Nioka, B. Chance, and A. G. Yodh, "Noninvasive diffuse optical measurement of blood flow and blood oxygenation for monitoring radiation therapy in patients with head and neck tumors: a pilot study," J. Biomed. Opt. **11**(6), 064021 (2006).
28. C. Zhou, R. Choe, N. Shah, T. Durduran, G. Yu, A. Durkin, D. Hsiang, R. Mehta, J. Butler, A. Cerussi, B. J. Tromberg, and A. G. Yodh, "Diffuse optical monitoring of blood flow and oxygenation in human breast cancer during early stages of neoadjuvant chemotherapy," J. Biomed. Opt. **12**(5), 051903 (2007).
29. H. Liu, Y. Gu, J. G. Kim, and R. P. Mason, "Near-infrared spectroscopy and imaging of tumor vascular oxygenation," Methods Enzymol. **386**, 349–378 (2004).

#157289 - $15.00 USD Received 28 Oct 2011; revised 15 Dec 2011; accepted 1 Jan 2012; published 4 Jan 2012

30. Y. Gu, W. R. Chen, M. Xia, S. W. Jeong, and H. Liu, "Effect of photothermal therapy on breast tumor vascular contents: noninvasive monitoring by near-infrared spectroscopy," Photochem. Photobiol. **81**(4), 1002–1009 (2005).
31. J. G. Kim, D. Zhao, Y. Song, A. Constantinescu, R. P. Mason, and H. Liu, "Interplay of tumor vascular oxygenation and tumor pO_2 observed using near-infrared spectroscopy, an oxygen needle electrode, and ^{19}F MR pO_2 mapping," J. Biomed. Opt. **8**(1), 53–62 (2003).
32. T. H. Pham, R. Hornung, M. W. Berns, Y. Tadir, and B. J. Tromberg, "Monitoring tumor response during photodynamic therapy using near-infrared photon-migration spectroscopy," Photochem. Photobiol. **73**(6), 669–677 (2001).
33. R. G. Steen, K. Kitagishi, and K. Morgan, "In vivo measurement of tumor blood oxygenation by near-infrared spectroscopy: immediate effects of pentobarbital overdose or carmustine treatment," J. Neurooncol. **22**(3), 209–220 (1994).
34. S. Fantini, S. A. Walker, M. A. Franceschini, M. Kaschke, P. M. Schlag, and K. T. Moesta, "Assessment of the size, position, and optical properties of breast tumors in vivo by noninvasive optical methods," Appl. Opt. **37**(10), 1982–1989 (1998).
35. Q. Zhu, S. Tannenbaum, and S. H. Kurtzman, "Optical tomography with ultrasound localization for breast cancer diagnosis and treatment monitoring," Surg. Oncol. Clin. N. Am. **16**(2), 307–321 (2007).
36. Q. Fang, J. Selb, S. A. Carp, G. Boverman, E. L. Miller, D. H. Brooks, R. H. Moore, D. B. Kopans, and D. A. Boas, "Combined optical and X-ray tomosynthesis breast imaging," Radiology **258**(1), 89–97 (2011).
37. B. J. Tromberg, B. W. Pogue, K. D. Paulsen, A. G. Yodh, D. A. Boas, and A. E. Cerussi, "Assessing the future of diffuse optical imaging technologies for breast cancer management," Med. Phys. **35**(6), 2443–2451 (2008).
38. H. Jiang, S. Ramesh, and M. Bartlett, "Combined optical and fluorescence imaging for breast cancer detection and diagnosis," Crit. Rev. Biomed. Eng. **28**(3 - 4), 371–375 (2000).
39. R. Choe, S. D. Konecky, A. Corlu, K. Lee, T. Durduran, D. R. Busch, S. Pathak, B. J. Czerniecki, J. Tchou, D. L. Fraker, A. Demichele, B. Chance, S. R. Arridge, M. Schweiger, J. P. Culver, M. D. Schnall, M. E. Putt, M. A. Rosen, and A. G. Yodh, "Differentiation of benign and malignant breast tumors by in-vivo three-dimensional parallel-plate diffuse optical tomography," J. Biomed. Opt. **14**(2), 024020 (2009).
40. Y. Shang, Y. Zhao, R. Cheng, L. Dong, D. Irwin, and G. Yu, "Portable optical tissue flow oximeter based on diffuse correlation spectroscopy," Opt. Lett. **34**(22), 3556–3558 (2009).
41. G. Yu, Y. Shang, Y. Zhao, R. Cheng, L. Dong, and S. P. Saha, "Intraoperative evaluation of revascularization effect on ischemic muscle hemodynamics using near-infrared diffuse optical spectroscopies," J. Biomed. Opt. **16**(2), 027004 (2011).
42. Y. Shang, R. Cheng, L. Dong, S. J. Ryan, S. P. Saha, and G. Yu, "Cerebral monitoring during carotid endarterectomy using near-infrared diffuse optical spectroscopies and electroencephalogram," Phys. Med. Biol. **56**(10), 3015–3032 (2011).
43. Y. Shang, L. Chen, M. Toborek, and G. Yu, "Diffuse optical monitoring of repeated cerebral ischemia in mice," Opt. Express **19**(21), 20301–20315 (2011).
44. D. A. Boas, L. E. Campbell, and A. G. Yodh, "Scattering and Imaging with Diffusing Temporal Field Correlations," Phys. Rev. Lett. **75**(9), 1855–1858 (1995).
45. D. A. Boas and A. G. Yodh, "Spatially varying dynamical properties of turbid media probed with diffusing temporal light correlation," J. Opt. Soc. Am. A **14**(1), 192–215 (1997).
46. D. A. Boas, "Diffuse photon probes of structural and dynamical properties of turbid media: theory and biomedical applications," Ph.D. dissertation (University of Pennsylvania, Philadelphia, 1996).
47. S. O. Rice, "Mathematical analysis of random noise," in *Noise and Stochastic Processes*, N. Wax, ed. (Dover, New York, 1954), p. 133.
48. C. Zhou, "In-vivo optical imaging and spectroscopy of cerebral hemodynamics," Ph.D. dissertation (University of Pennsylvania, Philadelphia, 2007).
49. D. T. Delpy, M. Cope, P. van der Zee, S. Arridge, S. Wray, and J. Wyatt, "Estimation of optical pathlength through tissue from direct time of flight measurement," Phys. Med. Biol. **33**(12), 1433–1442 (1988).
50. A. Duncan, J. H. Meek, M. Clemence, C. E. Elwell, L. Tyszczuk, M. Cope, and D. T. Delpy, "Optical pathlength measurements on adult head, calf and forearm and the head of the newborn infant using phase resolved optical spectroscopy," Phys. Med. Biol. **40**(2), 295–304 (1995).
51. J. G. Kim, M. Xia, and H. Liu, "Extinction coefficients of hemoglobin for near-infrared spectroscopy of tissue," IEEE Eng. Med. Biol. Mag. **24**(2), 118–121 (2005).
52. C. Cheung, J. P. Culver, K. Takahashi, J. H. Greenberg, and A. G. Yodh, "In vivo cerebrovascular measurement combining diffuse near-infrared absorption and correlation spectroscopies," Phys. Med. Biol. **46**(8), 2053–2065 (2001).
53. D. Irwin, L. Dong, Y. Shang, R. Cheng, M. Kudrimoti, S. D. Stevens, and G. Yu, "Influences of tissue absorption and scattering on diffuse correlation spectroscopy blood flow measurements," Biomed. Opt. Express **2**(7), 1969–1985 (2011).
54. Y. Shang, T. B. Symons, T. Durduran, A. G. Yodh, and G. Yu, "Effects of muscle fiber motion on diffuse correlation spectroscopy blood flow measurements during exercise," Biomed. Opt. Express **1**(2), 500–511 (2010).
55. NCI, *Response Evaluation Criteria in Solid Tumors (RECIST) Quick Reference* (NIH NCI, 2009).

#157289 - $15.00 USD Received 28 Oct 2011; revised 15 Dec 2011; accepted 1 Jan 2012; published 4 Jan 2012

1. Introduction

Head and neck cancer accounts for about 3 to 5% of all cancers in the United States [1]. These cancers are more common in men and in people over age 50 [2]. More than 90% of head and neck cancers are of squamous cell origin that line the mucosal tissues in the head and neck area, e.g., oral cavity, tonsils, larynx and hypopharynx [3]. Head and neck cancers very commonly spread to the lymph nodes of the neck. Radiation therapy is a principal modality in the treatment of head and neck cancers. According to the stage, size, and location of the tumors, radiation therapy may be combined with surgery, chemotherapy or both in the treatment of this disease [4]. Radiation therapy works by damaging the DNA of cancerous cells ultimately resulting in cell death. Radiation can also cause long-term changes in the vasculature mediated through inflammatory cytokines and other agents. When using x-ray beams for therapy, approximately two thirds of DNA damage is caused by free radical attack on the DNA [5]. The efficacy of radiation therapy with x rays is known to be dependent on tumor oxygen status. Under hypoxic conditions, the damage to DNA can be repaired more readily than under euoxic conditions where the damage is irreversible because of the interaction of tissue oxygen with free radicals [6,7]. Many tumors are hypoxic because of the high oxygen consumption by tumor cells and/or poor blood flow associated with tumor angiogenesis [6]. Studies using polarographic electrode have exhibited an increase of positive response to radiation therapy in tumors with high pretreatment oxygenation compared to poorly oxygenated tumors [8–12]. However, in these studies some well-oxygenated tumors failed to respond while some hypoxic tumors responded well, possibly due to the changes in tumor oxygen status during radiation treatment. Recent investigations using polarographic electrode, magnetic resonance imaging (MRI), dynamic computed tomography (CT) and ^{133}Xe clearance method have shown that tumor hemodynamic parameters changed over the period of radiation therapy and less-perfused tumors responded poorly [13–18]. Therefore, functional assessment of tumor oxygenation and blood flow changes during radiation therapy may help understand radiation pathology and holds potential for the prediction of therapy outcomes.

Tumor hemodynamics and metabolism, however, are not routinely measured during cancer therapy in clinic due to the lack of appropriate technologies. Several methods exist for the measurement of blood oxygenation and flow in tumors. The polarographic electrode method provides a point measurement of tumor oxygenation [8–12]. However it is invasive and often produces inconsistent results in highly heterogeneous tissues. Imaging modalities, such as positron emission tomography (PET) [19,20], dynamic CT [15,17,21,22], functional MRI (fMRI) [23] and perfusion MRI [13,16], provide structural and functional information about tumors but require large and costly instrumentation which limits their routine use in the clinic. Furthermore, these imaging modalities cannot measure tumor response in real time when radiation is being delivered into the tumor cells. Doppler ultrasound is a common clinical tool for functional measurement of blood flow within large vessels, but cannot probe tumor microvasculature [24].

Near-infrared (NIR) diffuse optical methods offer a noninvasive, portable, fast and low-cost alternative for repetitively monitoring tumor hemodynamics at the bedside when therapy is administered [25–39]. For example, Sunar et al. [27] have explored the use of a hybrid NIR diffuse optical instrument for noninvasive measurements of tumor hemodynamic responses to chemo-radiation therapy in patients with head and neck tumors. In their study, tumor blood flow and oxygenation were measured right before radiation treatment once a week throughout ~6 weeks of daily chemo-radiation therapy. Their patients exhibited significant flow and oxygenation changes during the first two weeks of treatment, suggesting a potential value of hemodynamic measurements for the early evaluation of treatment effects. These results are in reasonable agreement with other studies using perfusion MRI [16] and ^{133}Xe clearance method [18]. Furthermore, potential instant changes in tumor hemodynamics during radiation

#157289 - $15.00 USD Received 28 Oct 2011; revised 15 Dec 2011; accepted 1 Jan 2012; published 4 Jan 2012

delivery may also affect the treatment efficacy. For example, Yu et al. [25] have used a NIR diffuse correlation spectroscopy (DCS) for noninvasively monitoring tumor blood flow changes during photodynamic therapy (PDT). They observed a rapid flow decrease in murine tumors during PDT light illumination, leading to a poor long-term treatment efficacy. Similarly to radiation therapy, sufficient tissue oxygen must be presented during PDT to create singlet oxygen that kills tumor cells and vasculatures [25]. These previous results imply that continuous monitoring of tumor hemodynamics during radiation delivery may also assist in assessing treatment outcomes.

Very recently, a portable NIR DCS flow-oximeter has been developed and validated in our laboratory which can simultaneously measure tissue blood flow and oxygenation [40–43]. The present study is designed to test the feasibility of adapting this novel DCS flow-oximeter for noninvasive monitoring of tumor hemodynamics during radiation delivery. For this purpose, a customer-designed fiber-optic probe connected to the DCS flow-oximeter was placed directly on the surface of the radiologically/clinically involved cervical lymph node. The DCS flow-oximeter, located in the radiation treatment room, was remotely operated by a computer in the control room. From the early measurements, abnormal optical signals were observed when the optical device was placed in close proximity of the primary x-ray beams. Phantom tests were then designed to identify the source of artifacts. Thereafter, the radiation-generated artifacts were avoided by moving the optical device away from the primary x-ray beams. With the new experimental setup, eleven patients with head and neck tumors were successfully measured. To the best of our knowledge, these are the *first* noninvasive measurements of tumor hemodynamic changes during x-ray radiation delivery.

2. Methods and materials

2.1. Patient characteristics and treatment protocol

Twenty-three patients undergoing chemo-radiation therapy for head and neck tumors participated in this study with the signed consents approved by the University of Kentucky Institutional Review Board (IRB). Based on the source-detector (S-D) separation of 2.5 cm set in our fiber-optic probe (see Section 2.2), we included only Stage III-IVb SCCHN with a cervical tumor node larger than 2 cm detected by CT/PET/MRI scan and either clinically palpable or ultrasound defined. Patients with supraclavicular adenopathy were not enrolled as there was a possibility of the primary origin from other sites in the chest such as lung or esophagus. Radiotherapy in combination with traditional chemotherapy was applied on these patients. Each patient received daily fractional radiation over ~7 weeks. A total dose of 70 Gy was delivered in once daily fractions of 2 Gy. For chemotherapy, the cisplatin was given at 100 mg/m^2 on Day 1 and Day 22 of radiation. The role of chemotherapy (cisplatin) in head/neck cancer is to increase the incidence of double strand breaks (radiosensitization) and decrease the incidence of metastatic disease. During radiation delivery, the patient was immobilized on the treatment table with pre-molded plastic mask (see Fig. 1a and Fig. 1b). Radiation was delivered in the form of high-energy x-ray beams (6 MV) produced by a medical linear accelerator (Clinac 21EX, Varian Medical Systems, USA). The x-ray source was mounted on the end of an L-shaped gantry that can be rotated in a plane 360° around the longitudinal axis of the patient (see Fig. 1a). In this configuration, the x-ray source circumscribed a circle having a radius of 100 cm and always pointed toward the longitudinal patient axis. This allowed the x-ray beam to be focused to a point in the patient. Seven to nine source positions were approximately equally spaced over 360° around the patient. A typical treatment required approximately 15 minutes to complete, of which 3 to 4 minutes was actual radiation delivery. The radiation treatment consisted of a series of several short x-ray exposures (“beam-on”) followed by periods of no radiation (“beam-off”).

#157289 - $15.00 USD Received 28 Oct 2011; revised 15 Dec 2011; accepted 1 Jan 2012; published 4 Jan 2012

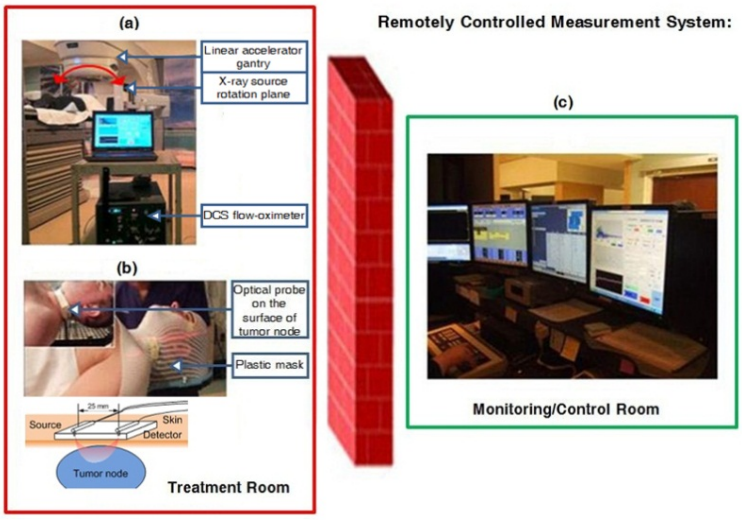

Fig. 1. A remotely operated DCS flow-oximeter system for monitoring head/neck tumor hemodynamics during radiation delivery. (a) A DCS flow-oximeter was placed away from the rotation plane of x-ray beams in the treatment room. (b) A fiber-optic probe connected to the DCS flow-oximeter was fixed on the surface of cervical tumor node using a pre-molded plastic mask. (c) A computer in the monitoring/control room was used to remotely operate the DCS flow-oximeter in the treatment room.

2.2. DCS flow-oximeter

Tumor blood flow and oxygenation changes during radiation delivery were monitored by a newly developed DCS flow-oximeter once a week over the 7-week treatment period. Details about the DCS flow-oximeter (see Fig. 1a) can be found elsewhere [40–43]. Briefly, long-coherence (>5 meters) NIR light emitted from two laser diodes (785 and 854 nm, ~100 mw, Crystalaser Inc., USA) enters the tissue alternately via two 200 μm diameter multimode source fibers that are tightly bundled together. The scattered light through the tissue is collected at a distance of 2.5 cm from the source fibers using a 5.6 μm diameter single-mode detector fiber connected to an avalanche photodiode (APD, PerkinElmer Inc., Canada). The APD measures light intensity (photon count rate) fluctuations from a single speckle area [~25 μm^2 ($\pi \times (5.6/2)^2$)] on the tissue surface and its output is fed into a correlator board (correlator.com, USA) for computing the light intensity temporal autocorrelation function [44–46]:

$$g_2(r, \tau) = \frac{\langle I(r,t) \cdot I(r, t+\tau) \rangle}{\langle I \rangle^2}$$

Here I(r, t) is the detected light intensity at position r and time t, $\langle \cdots \rangle$ denotes a time average, and τ is the autocorrelation delay time. The electric field temporal autocorrelation function $G_1(r, \tau)$ can be derived from the measured $g_2(r, \tau)$ using the Siegert relation: $g_2(r, \tau) = 1 + \beta \frac{|G_1(r, \tau)|^2}{\langle I \rangle^2} = 1 + \beta |g_1(r, \tau)|^2$ [47]. Here $g_1(r, \tau) = \frac{|G_1(r, \tau)|}{\langle I \rangle}$ is the normalized electric field autocorrelation function, and β is a coherent factor depending mainly on the laser coherence and detection optics and is inversely proportional to the number of speckle size. Considering the two orthogonal polarization modes collected from the single-mode detector fiber, the maximum β value should be ~0.5 [48]. When a polarizer is placed in front of the detection fiber, a β value of ~1 can be achieved. Note that the biological system studied must be assumed ergodic when applying the Siegert relation. The approximation of biological

#157289 - $15.00 USD Received 28 Oct 2011; revised 15 Dec 2011; accepted 1 Jan 2012; published 4 Jan 2012

tissues as an ergodic system may cause DCS measurement errors [46]. However, previous validation studies have shown that DCS flow measurements are in good agreement with other microvasculature flow measurement techniques [25,27], suggesting such potential errors are not significant.

The $G_1(r, \tau)$ satisfies the correlation diffusion equation in highly scattering media [44–46]. For semi-infinite homogeneous tissue, the analytical solution of $G_1(r, \tau)$ is a function of the mean-square displacement $<\Delta r^2(\tau)>$ of moving scatterers in tissue (primarily red blood cells). For the case of diffusive motion, $<\Delta r^2(\tau)> = 6D_B\tau$, where D_B is an *effective* diffusion coefficient of the moving red blood cells. An α term (0 to 1) is added to account for not all scatterers in tissue being dynamic and is defined as the ratio of moving scatterers to total scatterers (static + dynamic). The combined term, αD_B, is referred to as the blood flow index in biological tissues and is commonly used to calculate the relative blood flow (rBF) compared to the baseline flow index before physiological changes. The αD_B and β are derived by fitting the measured autocorrelation function to the analytical solution of $g_2(r, \tau)$.

The oxygenation information is obtained by recording the light intensities at two wavelengths (785 and 854 nm) [40–43]. These two wavelengths were chosen based on the lasers available at the time when the instrument was built. Optimization of wavelengths will be the subject of future work. The changes of oxygenated hemoglobin concentration (ΔHbO_2) and deoxygenated hemoglobin concentration (ΔHb) relative to their baseline values before treatment are calculated using a "differential pathlength method," based on the modified Beer-Lambert Law [49]. The modified Beer-Lambert law incorporates the increased optical pathlength due to tissue scattering. A differential pathelength factor (DPF), the ratio of the mean photon pathlength to the physical separation of the source and detector, is introduced to account for the pathlength increase. The ΔHbO_2 and ΔHb are derived from the measured changes in light intensities at the two wavelengths which depend on the extinction coefficients and DPF values at the corresponding wavelengths. The extinction coefficients and DPF values are determined based on the literature [50,51].

2.3. Remotely operated optical measurements during radiation delivery

A customer-designed fiber-optic probe was taped on the surface of the radiologically/clinically involved cervical lymph node (see Fig. 1b) using Elastikon tape (Johnson & Johnson Inc., USA) for tumor blood flow and oxygenation measurements. The optical probe consisted of source and detector fibers (at a separation of 2.5 cm) whose tips were bent 90° and held by a soft-foam pad. The nonmetallic optical fibers and the soft-foam pad are low-density, low atomic number materials which have negligible attenuation effects on the x-ray beam. A standard head/shoulder plastic immobilization mask (WFR/Aquaplast Corp., USA) was molded around the pre-positioned optical probe to ensure proper probe placement during subsequent treatment sessions (see Fig. 1b). The optical probes and DCS flow-oximeter device were kept inside the treatment room during radiation delivery and the laptop console was remotely operated by a computer located in the monitoring/control room (See Fig. 1c). The two computers worked under the "Remote Desktop Connect" mode in the Microsoft Windows Operating System and communicated through the internal network in the clinic. Using this real-time monitoring system, the optical measurements can be precisely timed with the presence or absence of the x-ray beam.

From the early optical measurements in some patients, abnormal values of β (>0.5) and αD_B were observed for some x-ray beam positions. The occurrence of the artifacts depended on the angle of the x-ray beams as well as the location of optical device. We suspect that scattered x rays were interacting directly with the photodiodes generating spurious signals. These signal perturbations were apparently responsible for the measurement artifacts in autocorrelation functions. To confirm the source of these artifacts, phantom tests were performed (see Section 2.4) under the same radiation conditions used for the patient treatments.

#157289 - $15.00 USD Received 28 Oct 2011; revised 15 Dec 2011; accepted 1 Jan 2012; published 4 Jan 2012

2.4. Phantom tests to identify optical measurement artifacts

Tissue-like liquid phantoms have been commonly used for instrument calibration and experimental validation of DCS techniques [46,48,52,53]. For this study, the experimental phantom was prepared by filling a cylindrical tank with the mixture of distilled water, India ink (Black India 44201, Higgins, USA) and Intralipid (Fresenius Kabi, Sweden). India ink was used to determine the absorption coefficient μ_a while Intralipid provided particle Brownian motion (flow) and control of the reduced scattering coefficient μ_s'. We set $\mu_a = 0.12$ cm^{-1} and $\mu_s' = 8$ cm^{-1} at 785 nm to mimic the property of real tissues [53]. The Intralipid phantom provided a homogeneous tissue model with controlled optical properties and constant particle flow, which should not be changed by the x rays. In addition, using tissue phantom can avoid some other potential artifacts (e.g., motion artifacts) that may occur in the patient measurements [54].

The set up for the phantom test was similar to that for patient measurements shown in Fig. 1, except that the patient was replaced with the liquid phantom contained by a cylindrical tank. During the beam-on interval, the x-ray beam was turned on continually and rotated around the liquid phantom over 360 degrees. The fiber-optic probe was secured in contact with the phantom surface using a customer-designed holder. The DCS flow-oximeter device was set up in two locations inside the treatment room; one was close to the x-ray beam plane so that the optical device was subjected to a significant fluence of scattered x rays and another was several meters away from the x-ray beam plane. This arrangement approximated the two extreme positions in a typical patient treatment delivery. The radiation beam energy (6 MV) used for the phantom tests was same for the patient treatments (see Section 2.3).

2.5. Optical data analysis and presentation

Although 23 patients were measured, 12 patient data were excluded for data analysis as their optical measurements were thought to be contaminated by scattered x rays. The data exclusion was based on the abnormal β value (>0.5). Details about the tumors, optical measurements (without artifacts), and treatment outcomes of the eleven male patients aged 53 to 74 years are listed in Table 1. Patients with unknown primary cancers (#6 and #8) were treated as head/neck cancers based on nodal stage of disease with primary origin suspected in the tonsil or the base of tongue. The Response Evaluation Criteria in Solid Tumors (RECIST) [55] were used to define the tumor response to chemo-radiation therapy. For example, a complete response (CR) indicates the disappearance of all target lesions and a partial response (PR) represents at least a 30% decrease in the sum of the longest diameter of target lesions. Note that even though some lymph nodes persisted 12 weeks post-treatment (see the post-radiation tumor volumes of Patients #2, #4, #7 listed in Table 1), they were physiologically normal; the PET was not showing activity and no further treatment was needed. The metastatic adenopathy in Patient #4 was in the upper neck. The optical measurements over the entire treatment course were not always available for each individual due to the patient related events such as side effects of treatment, fatigue, non-compliance with chemo-radiation regimen or due to time constraints of obtaining measurements and modification of treatment schedules as a consequence of temporary breakdown in radiation therapy equipment.

Since DCS flow signals are not sensitive to variation in the wavelength [40,53], blood flow data obtained from one wavelength (785 nm) are presented in this study. The time courses of blood flow and oxygenation data are normalized to their baseline values right before the radiation delivery, respectively. More specifically, rBF represents the blood flow change relative to its baseline (assigned to be "1"), and the ΔHbO_2 and ΔHb are the dynamic changes in oxygenated and deoxygenated hemoglobin concentrations relative to their baselines (assigned to be "0"). The rBF, ΔHbO_2 and ΔHb during the fractional radiation deliveries (beam-on intervals) or between the fractional deliveries (beam-off intervals) are

#157289 - $15.00 USD Received 28 Oct 2011; revised 15 Dec 2011; accepted 1 Jan 2012; published 4 Jan 2012

Table 1. Characteristics of tumors, optical measurements, and treatment outcomes[a]

Pat. No.	Primary site	TNM	Optical measurements over the 7-week treatment period							Tumor node volume (cm^3)		Tumor responses		
			1	2	3	4	5	6	7	Pre-RT	Post-RT	Primary	LN	Overall
1	Tonsil	T2N2cM0	A	A	A	A				34	6	CR	CR	CR
2	BOT	T3N2cM0	A	A						57.9	35	PR	CR*	PR
3	BOT	T1N2bM0	A	A						27	1.32	CR	CR	CR
4	BOT	T2N2cM0	A							90	27	CR	CR	CR but metastasis developed
5	Tonsil	T1N2bM0	A							24	1.3	CR	CR	CR
6	Unknown	TxN3M0	A	A	A	A	A	A	A	18	0	CR	CR	CR
7	BOT	T2N2cM0	A	A	A	A	A	A		28	13	CR	CR	CR
8	Unknown	TxN2bM0	A	A	E	E	E	A	A	14.6	1	CR	CR	CR
9	Larynx	T4aN2aM0	A	A	A					44.1	1	CR	CR	CR
10	BOT	T3N2cM0	A	A		A	A	A	A	14	0	CR	CR	CR
11	Larynx	T3N2cM0	A	A	A	A		A	A	16	0	CR	CR	CR

[a]Abbreviations: Pat. = Patient, BOT = Base of Tongue, TNM = Tumor, Node, and Metastasis stage, RT = Radiation Therapy, A = Data Available, E = Data Excluded (unstable baseline of optical measurements), LN = Lymph Node, CR = Complete Response, PR = Partial Response

*indicates that the patient underwent a neck dissection after Chemo-RT and had persistent radiological finding suspicious for persistent disease but the pathology specimen did not show viable tumor.

averaged separately for assessing the instant response to radiation delivery in each individual. The averaged hemodynamic changes over patients at multiple weeks generate the dynamic variation trends of rBF, ΔHbO_2 and ΔHb over the 7-week treatment period. The average hemodynamic responses over subjects are presented as means ± standard errors (error bars) in figures. For statistical analyses, significance is tested using the paired t-test. The criterion for significance is $p < 0.05$.

Results

3.1. Phantom tests

Figure 2 shows the optical measurement data at the wavelength of 785 nm from the phantom test when the DCS flow-oximeter was placed close to the x-ray beam plane. During the test,

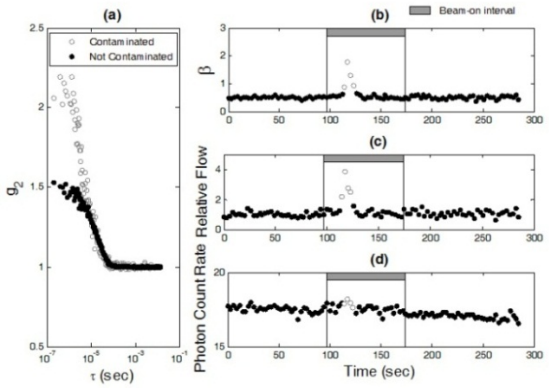

Fig. 2. The phantom test results to verify the source of optical measurement artifacts. (a) Two autocorrelation curves (g_2) were collected at the time points of 117 (contaminated) and 55 (not contaminated) (sec), respectively. The measured autocorrelation curve (empty circles) was contaminated by scattered x rays, resulting in an abnormal increase in β. (b) The appearance of abnormal increases in β (>0.5, empty circles) depended on the direction/angle of the radiation beam that rotated 360° around the phantom. (c) The x-ray beam induced abnormal increases in relative flow (empty circles) derived from the autocorrelation curves. (d) The x-ray beam induced slight increases in detected photon count rate (× 10^3 photons/s) (empty circles).

#157289 - $15.00 USD Received 28 Oct 2011; revised 15 Dec 2011; accepted 1 Jan 2012; published 4 Jan 2012

the x-ray beam was rotated around the liquid phantom over 360 degrees. When the x-ray beam was directed toward the optical device, abnormal correlation curves (g_2) were obtained (see an example shown in Fig. 2a) leading to large increases in β (>0.5, see Fig. 2b) and αD_B (see Fig. 2c) as well as slight increases in detected photon count rate (see Fig. 2d). When the DCS flow-oximeter device was moved away from the rotation plane of the x-ray beams, the optical measurements became normal for all beam directions. Similar results at the wavelength of 854 nm were also found during the phantom test (data are not shown). Notice that in this study β (Fig. 2b) and αD_B (Fig. 2c) were derived by fitting the measured autocorrelation function curve g_2 (Fig. 2a), as mentioned in Section 2.2. However, β can be also estimated based on the Siegert relation using the measured g_2 data (Fig. 2a) at earliest τ and letting the normalized autocorrelation function $g_1 \approx 1$, i.e., $\beta = g_2(\tau \approx 0) - 1$ (Fig. 2b) [53].

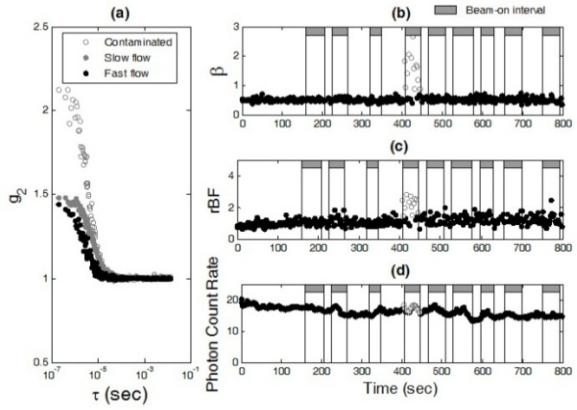

Fig. 3. The *in vivo* measurement results for the investigation of optical measurement artifacts induced by scattered x rays. (a) Three autocorrelation curves (g_2) were collected at the time points of 417 (contaminated), 99 (slow flow), and 724 (fast flow) (sec), respectively. Similar to the phantom test results (see Fig. 2a), scattered x rays contaminated the measured autocorrelation curves (empty circles). For the data without contaminations (solid circles), the decay rate of autocorrelation curves depended on the level of blood flow; g_2 decayed faster when blood flow was faster (black solid circles). As expected, β (can be estimated using the measured g_2 data at earliest τ) was independent of blood flow changes when there were no x-ray induced artifacts. (b) Scattered x rays created abnormal increases in β (>0.5, empty circles) depending on the direction/angle of radiation beam. (c) The x-ray beam introduced abnormal increases in blood flow (empty circles) derived from the autocorrelation curves. (d) The x-ray beam induced minor variations in detected photon count rate ($\times 10^3$ photons/s) (empty circles).

3.2. In vivo optical measurements

Artifacts were also observed in some optical measurements of tumor hemodynamics for some x-ray beam directions. Figure 3 shows the typical contaminated optical data measured at the wavelength of 785 nm during a fractional radiation treatment. Similar to the phantom test results, abnormal correlation curves as well as the increases in β (>0.5) and blood flow index (αD_B) were observed (see Fig. 3a, 3b, and 3c) when the optical device was subjected to significantly scattered x rays. This effect also induced minor variations in detected photon count rate (see Fig. 3d). Similar artifacts were also observed at the wavelength of 854 nm (data are not shown). These results are consistent with the findings from the phantom tests (see Section 3.1).

After identifying the source of radiation artifacts, we modified the optical measurements to minimize these effects. A new fiber-optic probe was constructed using the source and detector fibers with a length longer than 5 meters. The optical device connected with the new probe was placed approximately 3 meters from the rotation plane of the x-ray beams. The longer fiber cable allowed the DCS detector assembly to be moved much further away from the

#157289 - $15.00 USD Received 28 Oct 2011; revised 15 Dec 2011; accepted 1 Jan 2012; published 4 Jan 2012

primary beam plane so that the impact of scattered x rays on the detector was minimized. Thereafter, using the new measurement configuration no artifacts (i.e., abnormal β and αD_B) were observed in the optical data. Figure 4 shows the typical responses of rBF, ΔHb and ΔHbO_2 during radiation delivery measured from one patient (#6) at two different weeks (Week 1 and Week 4). The values of β throughout the treatment period were stable and approximately equal to 0.5 (see Fig. 4a and Fig. 4b), indicating no artifacts involved in the optical measurements. A gradual increase in rBF was observed at Week 1 (see Fig. 4c), but not at Week 4 (see Fig. 4d). Variations in ΔHb (see Fig. 4e and Fig. 4f) and ΔHbO_2 (see Fig. 4g and Fig. 4h) were also found at both weeks. There were no obvious differences in tumor hemodynamic responses (i.e., rBF, ΔHb and ΔHbO_2) between the intervals of x-ray beam-on and beam-off.

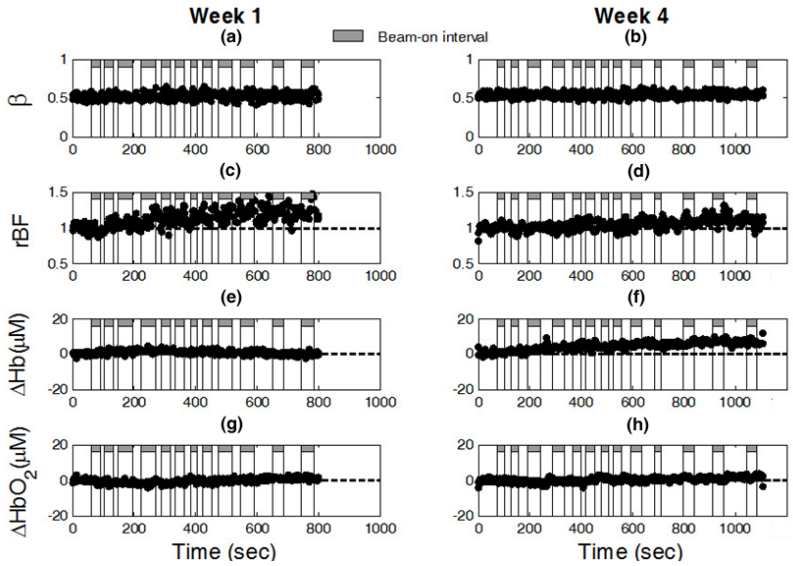

Fig. 4. The *in vivo* optical measurement results without x-ray induced artifacts during radiation delivery from one patient (#6) at Week 1 (left panel) and Week 4 (right panel). As expected, β ((a) and (b)) was stable throughout the fractional radiation deliveries and independent of blood flow changes. The typical responses of rBF ((c) and (d)), ΔHb ((e) and (f)), and ΔHbO_2 ((g) and (h)) were continuously monitored by the DCS flow-oximeter during radiation delivery.

3.3. Averaged hemodynamic responses over patients

Figure 5 shows the averaged dynamic changes in rBF, ΔHb, and ΔHbO_2 over the 11 patients at different weeks. The numbers of patients with valid optical data (without artifacts) are labeled at each week in Fig. 5a. On average, there were no significant differences in most of the measured hemodynamic variables (i.e., rBF, ΔHb, ΔHbO_2) between the intervals of x-ray beam-on and beam-off, except that a small but significant difference in ΔHbO_2 (-0.29 ± 0.12 μM, $p = 0.03$) was observed between the x-ray beam-on and beam-off at Week 1 (see Fig. 5c). However, the changes in ΔHbO_2 during radiation delivery at Week 1 for both beam-on and beam-off were insignificant compared to their baseline values, respectively. As a result, the averaged ΔHbO_2 changes including both beam-on and beam-off data at Week 1 were also insignificant. Therefore, the hemodynamic changes were believed to be induced by an accumulated effect of the fractional radiation dose over the entire period of radiation delivery. Thus, we calculated the individual means of hemodynamic responses (i.e., rBF, ΔHb and ΔHbO_2) over the entire course of radiation treatment including both beam-on and beam-off intervals. The calculated average hemodynamic results over the 11 patients are listed in Table 2. Although variations in rBF during radiation delivery were observed over the 7-week

#157289 - $15.00 USD Received 28 Oct 2011; revised 15 Dec 2011; accepted 1 Jan 2012; published 4 Jan 2012

treatment period, only the change at the first week (1.11 ± 0.03) was significant (p = 0.003) compared to its baseline before treatment. By contrast, the variations in both ΔHb and ΔHbO_2 over the treatment periods were not statistically significant.

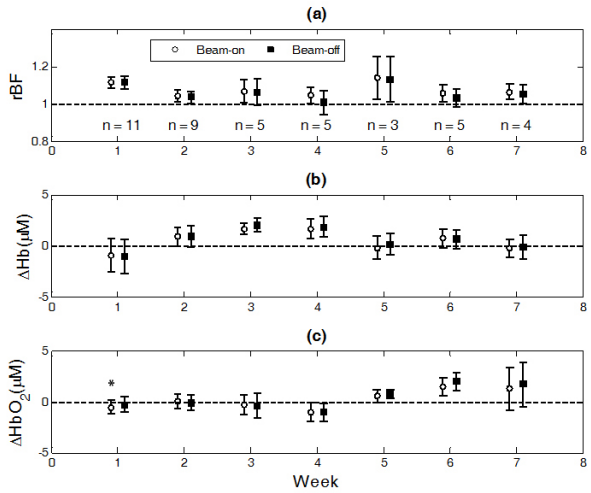

Fig. 5. The averaged dynamic changes in rBF (a), ΔHb (b) and ΔHbO_2 (c) over the 11 patients at different weeks. Data obtained during the fractional radiation deliveries (beam-on intervals) or between the fractional deliveries (beam-off intervals) were averaged separately. A small but significant difference in ΔHbO_2 (–0.29 ± 0.12 μM) was observed between the x-ray beam-on and beam-off at Week 1 (* represents p = 0.03).

Table 2. Overall changes (mean ± standard error) in rBF, ΔHb and ΔHbO_2 over 11 patients at different weeks

Week	1	2	3	4	5	6	7
No. of patients	11	9	5	5	3	5	4
rBF	1.11 ± 0.03**	1.04 ± 0.03	1.07 ± 0.06	1.03 ± 0.05	1.13 ± 0.12	1.05 ± 0.04	1.06 ± 0.04
ΔHb (μM)	–0.96 ± 1.66	0.91 ± 1.00	1.82 ± 0.58	1.77 ± 0.97	0.05 ± 1.10	0.71 ± 0.92	–0.21 ± 1.02
ΔHbO_2 (μM)	–0.44 ± 0.70	0.00 ± 0.69	–0.36 ± 1.07	–0.97 ± 0.87	0.67 ± 0.54	1.66 ± 0.85	1.46 ± 2.14

**represents p = 0.003.

4. Discussion and conclusions

Previous studies have shown that the quantification of pretreatment tumor hemodynamic status holds potential for the prediction of radiation treatment outcomes [8–12]. Real-time monitoring of tumor hemodynamic changes during radiation delivery may provide additional information for better evaluation of treatment effects. Such information may be useful for pretreatment planning or early adjustment of treatment modalities. For example, if correlated with poor treatment outcomes, highly hypoxic tumors identified before treatment may be directly referred for surgery instead of radiotherapy. Non-responders to radiotherapy, if identified by early tumor hemodynamic responses (e.g., within the first two weeks of treatment), may be administered alternative neoadjuvant therapy and/or referred for surgery. Such management can avoid delays in the selection of appropriate treatment modalities, thus potentially reducing patient complications due to radiotherapy that is either unnecessary or not efficacious.

However, currently available imaging modalities (e.g., fMRI, PET and Dynamic CT) cannot be used at the bedside of clinical treatment rooms to perform real-time monitoring during radiation delivery. Although NIR diffuse optical techniques have been used as bedside

#157289 - $15.00 USD Received 28 Oct 2011; revised 15 Dec 2011; accepted 1 Jan 2012; published 4 Jan 2012

monitoring tools in many clinical studies [25–39], they have not been applied to patients inside the radiation treatment room. The challenges to adapt the optical techniques for use during radiation delivery include installing the optical probe properly on the surface of tumor node, operating the optical device from a separated control room, and avoiding the potential interference between the scattered x rays and optical measurements. In the present study several crucial steps were taken to adapt the DCS flow-oximeter for the use of monitoring tumor blood flow and oxygenation during radiation delivery. A pre-molded plastic mask was made to hold the optical probe in a proper contact with the tumor nodal mass (see Fig. 1a and Fig. 1b) throughout the treatment period for reducing the motion artifacts to optical measurements. Two computers located separately in the treatment and control rooms communicated through the internal network, enabling to remotely operate the DCS flow-oximeter (see Fig. 1c). Finally, tissue phantom tests were conducted to determine the source of optical measurement artifacts (i.e., abnormal β and αD_B) observed in the patient measurements during radiation delivery.

As described early in Section 2.2, β depends mainly on the detection optics, and the maximum β value should be ~0.5 when using a single-mode fiber to detect the speckle fluctuations [48]. However, abnormal high values of β (>0.5) were observed during radiation delivery in both phantom (see Fig. 2) and patient (see Fig. 3) measurements when the optical device was placed close to the rotation plane of x-ray beams. When the DCS flow-oximeter device was moved away from the x-ray beams, the optical measurements became normal throughout the entire treatment period (see Fig. 4). These findings suggest that the observed artifacts were generated by the scattered x rays interacting directly with the optical detector and they can be eliminated by simply moving the optical device (detector) away from the radiation beams.

After moving the optical device out of the x-ray beams, we have successfully collected valid optical data (without artifacts) from 11 patients during x-ray delivery. Large inter-patient variations in tumor hemodynamic responses were observed during radiation delivery (see the large error bars in Fig. 5). On average (see Table 2), a significant increase in tumor blood flow during radiation delivery was observed at the first week of treatment, which may be a physiologic response to hypoxia created by radiation oxygen consumption. Similar increases in blood flow were previously observed in tumors during the early period of PDT delivery [25]. This regulation ability in blood flow seemed to decline with the progress of weekly treatments. Interestingly, only small and insignificant changes were found in tumor blood oxygenation (ΔHb and ΔHbO_2) during radiation delivery over the 7-week treatment period (see Table 2). The absence of substantial tumor oxygenation changes suggested that oxygen utilizations in tumors during the short period of fractional radiation deliveries (3 to 4 minutes) were either minimal or balanced by other effects such as blood flow regulation. Clarification of the reasons for limited oxygenation changes during radiation delivery will require separate investigations. Oxygenation changes during radiation therapy may be due to the reassortment of the cells in the cell cycle, revascularization, repopulation of the tumor cells and cell kill. As these issues were not being measured it is outside the purview of the present study.

Although the present investigation has yielded preliminary findings, some study limitations need to be noted. Firstly, the continuous-wave (CW) DCS flow-oximeter measures only the relative changes of tumor hemodynamics during radiation delivery. It is surely possible that the absolute baseline values of tumor hemodynamics are different among patients before treatment [53] and can be changed by the fractional radiation treatments over the treatment period [27]. Furthermore, the CW DCS flow-oximeter used in this study cannot quantify tissue scattering changes during treatment. However, results from the previous study [27] using a frequency-domain device showed that only ~5% changes in tumor scattering coefficient (μ_s') were observed over several weeks of fractionated radiation treatment. According to our recent study on the influences of μ_s' to DCS measurement [53], this small amount of μ_s' variation should not significantly affect our flow results. The second limitation

#157289 - $15.00 USD Received 28 Oct 2011; revised 15 Dec 2011; accepted 1 Jan 2012; published 4 Jan 2012

concerns the small number of patients (n = 11) and availability of the optical measurements over the entire course of treatment (see Table 1). A large pool of patients and optical data would increase the statistical power of measurement results. Lastly, the treatment outcomes from the patients need to be correlated with tumor hemodynamic responses to determine the prognostic value of optical measurements. However, all eleven patients involved in this study demonstrate consistent treatment outcomes (i.e., a complete response to radiation treatment) in the measured cervical lymph nodes (see Table 1), making it impossible to investigate the correlations between tumor hemodynamic responses and clinical outcomes. To overcome these limitations of the present study, we have recently combined the DCS device with a commercial frequency-domain tissue-oximeter (Imagent, ISS Inc. USA) that can measure the absolute values of tumor optical properties and tumor oxygenation [53]. We will use this hybrid instrument to quantify the absolute values of tumor hemodynamics during radiation treatment. More patients are being recruited and clinical outcomes continue to be collected.

Although there is much work to be done, our pilot study results suggest that tumor hemodynamic changes during radiation delivery can be optically detected using the DCS flow-oximeter without being overly burdensome on patients. The unique remotely operated optical system developed in this study has potential to be used in other therapeutic/diagnostic rooms (e.g., CT) where operators are not allowed to stay. It is our hope that real-time monitoring of tumor hemodynamic changes during radiation delivery integrated with the pretreatment absolute measurements of tumor blood flow and oxygenation will provide best information for the early prediction of cancer treatment outcomes.

Acknowledgments

This work was supported by the grant from NIH R01 CA149274 (G.Y.). We thank Daniel Kameny, Jacqueline Sims, Karen Meekins, and Laura Reichel for their assistance in recruitment of patients.

#157289 - $15.00 USD Received 28 Oct 2011; revised 15 Dec 2011; accepted 1 Jan 2012; published 4 Jan 2012